Strength Prediction of Rectangular FRP-Reinforced Concrete Columns Under Eccentric Loading

Nam Nguyen Van[1], Hiep Dang Vu[2], Duy Nguyen Phan[1,*]

[1]Faculty of Civil Engineering, Industrial University of Ho Chi Minh City, Ho Chi Minh City, Vietnam

[2]Faculty of Civil Engineering, Hanoi Architectural University, Hanoi City, Vietnam

Received 09 May 2025; received in revised form 31 August 2025; accepted 24 September 2025

DOI: https://doi.org/10.46604/aiti.2025.15124

Abstract

This study aims to develop an analytical model for evaluating the load-carrying capacity of rectangular fiber-reinforced polymer (FRP) reinforced concrete columns under eccentric loading. In the proposed model, the contribution of FRP bars in compression is considered, with their compressive strength estimated as a fraction of tensile strength. Meanwhile, the effects of confinement, tension stiffening, and second-order effects are conservatively neglected. Two main failure modes, namely concrete crushing and FRP rupture, are distinguished by the balanced failure condition. This model applies strain compatibility with the plane section and constitutive laws to derive stress-strain distributions across the cross-section. Then, the model is validated against 91 experimental results covering diverse sections, strengths, and eccentricities (e/h = 0.1-1.0), showing high accuracy (mean: 0.932; RMSE: 0.154; COV: 22.9%; SD: 0.145; r: 0.84) and outperforming ACI CODE-440.11. Analysis results also show that compressive FRP reinforcement contributed between 0.94% and 22.3% to the column strength.

Keywords: FRP, concrete column, eccentricity, analytical method

1. Introduction

Steel-reinforced concrete (RC) structures are extensively used in buildings, transportation infrastructure, including roads and railways, hydraulic structures, and marine applications due to their many advantages. However, steel corrosion in harsh environments reduces the durability and lifespan of RC structures. Fiber-Reinforced Polymer (FRP) reinforcement for concrete structures has been under development since the 1960s and has gradually become a viable alternative to traditional steel reinforcement in specific environments, owing to its high tensile strength, corrosion resistance, electromagnetic neutrality, electrical insulation, and high strength-to-weight ratio [1]. Common FRP rebar types include carbon FRP (CFRP), basalt FRP (BFRP), aramid FRP (AFRP), and glass FRP (GFRP) [1-2]. Despite these advantages, FRP-RC structures have not yet been widely adopted worldwide due to several limitations: only a few countries have developed design standards; the structural behavior of FRP-RC is not fully understood; theoretical models are still being improved; and the cost of FRP bars remains relatively high. As a result, research on FRP-RC structures continues to attract significant attention.

Unlike traditional steel reinforcement, which exhibits good tensile and compressive strength as well as a high modulus of elasticity, FRP reinforcement has significantly lower compressive strength compared to its tensile capacity. It also has a lower elastic modulus and behaves in a brittle manner without yielding. As a result, the structural behavior and design methodology of FRP-RC columns differ markedly from those of conventional RC columns. Consequently, the study of the behavior of FRP-RC columns has attracted considerable interest from researchers worldwide [3].

* Corresponding author. E-mail address: nguyenphanduy@iuh.edu.vn

Although most existing research on FRP-RC columns focuses on axial loading, real-world conditions rarely involve pure axial forces. Eccentricity arising from load misalignment, second-order effects, or construction imperfections leads to significant moment-axial interaction, which is especially critical in FRP-RC columns due to the linear-elastic behavior of FRP bars. In contrast, concentrically loaded FRP-RC columns have been more extensively studied, and their behavior is relatively simple and, in many aspects, analogous to that of conventional steel-RC columns. Several analytical models have been proposed for such cases, often adapting existing design formulas developed for concentrically loaded steel-RC columns [4]. However, under eccentric loading, FRP-RC columns exhibit more complex nonlinear behavior due to cracking, lack of yielding, and tension-compression interactions, which necessitate a dedicated modeling approach to ensure accurate predictions and safe design.

Studies show that FRP-RC columns exhibit distinct behavior compared to steel-RC columns under eccentric compression, primarily due to linear-elastic behavior and lower modulus of elasticity of FRP reinforcement [5]. Unlike steel-RC columns, which display ductile yielding, FRP-RC columns show brittle failure after peak load due to the absence of a yield point [6]. GFRP- and BFRP-RC columns have 17-30% lower capacities than steel RC columns, whereas CFRP-RC columns have a load-carrying capacity averaging 7% lower load-carrying capacity [4, 7]. FRP-RC columns experience larger longitudinal deformations but smaller crack widths. In terms of failure modes, FRP-RC columns predominantly fail by concrete crushing under concentric and low-eccentricity loading, often accompanied by cover spalling or bar kinking [4]. At moderate eccentricities, failure transitions to compression-dominated or flexural-compression modes, with flexural cracking and gradual concrete degradation [8]. High-eccentricity loading results in flexural-tension failure with tension-side cracks and excessive deformations [9].

Research indicates that the compressive strength of FRP bars ranges from 10% to 86% of their tensile strength, depending on the fiber type [10]. While the compressive modulus of elasticity of FRP reinforcement is relatively close to its tensile modulus (with a ratio between 0.97 and 1.20) [3, 10], the much lower compressive strength significantly limits its effectiveness in compressive members such as columns. Studies indicate that increasing the FRP reinforcement ratio in FRP-RC columns from 1% to 3.8% enhances load-carrying capacity by 5-35%, particularly at high eccentricities [9, 11]. An increase in FRP reinforcement ratio also enhances flexural stiffness and reduces post-peak decay [9]. Despite their limited compressive strength, FRP bars still contribute meaningfully to the load-carrying capacity of FRP-RC columns: approximately 3-15% for GFRP, 6-19% for CFRP, and around 11% for BFRP, compared to 6.5-36% for steel reinforcement [4, 8]. As a result, many authors recommend accounting for the contribution of compressive FRP reinforcement in design methods [3, 12].

Similar to steel-RC columns, the load-carrying capacity of FRP-RC columns under eccentric compression depends on several factors, including material characteristics, longitudinal reinforcement ratio, eccentricity, slenderness, and confinement effect of transverse reinforcement. Slenderness amplifies second-order effects (P-Δ effect) in FRP-RC, resulting in greater strength degradation and larger deformations compared to steel-RC columns [5, 13]. Short FRP-RC columns (slenderness ratio $\leq$ 18) show minimal second-order effects (4-10% of total moment), allowing simplified design without considering these effects [8]. However, slender FRP-RC columns require careful consideration of second-order effects [7]. Transverse reinforcement, such as GFRP or CFRP ties and spirals, enhances confinement and prevents longitudinal bar buckling [14-15]. Reducing tie spacing improves ductility, confinement, and residual strength, and can also shift the failure mode of the column from brittle to more ductile behavior [14-16]. Tightly spaced ties tend to cause failure by concrete crushing or rupture of transverse reinforcement, whereas wider tie spacing often leads to longitudinal bar buckling [14].

Current design codes like ACI 440.1R-15 [17], ACI CODE-440.11-22 [18], CSA S806:2012:R2017 [19], and SP 295.1325800.2017 [20] utilize equilibrium equations and strain compatibility principles, along with an equivalent concrete stress block, to calculate the axial load-carrying capacity of eccentrically loaded FRP-RC columns. In these methods, the contribution of FRP bars located in the compression zone is commonly neglected and is not considered in the load-carrying

mechanism. While this assumption simplifies design and ensures safety, it often results in conservative predictions and underestimation of the actual structural capacity [4, 15]. To address this, many researchers have proposed alternative methods for calculating the load-carrying capacity of FRP-RC columns under eccentric compression.

Sharbatdar [1] developed a plane section analysis method, validated through experiments on CFRP-RC columns, focusing on concrete crushing as the primary failure mode. Choo et al. [5] employed numerical integration to derive axial load-moment-curvature relationships, accounting for slenderness effects and recommending a reduced slenderness ratio (17 vs. 22) for non-sway frames. Zadeh and Nanni [21] adapted ACI 318-11 principles, using strain compatibility and force equilibrium to construct interaction diagrams for GFRP-RC columns. Elchalakani et al. [15] modified AS 3600, integrating Mander's confinement model and GFRP properties to develop moment-axial load interaction diagrams. Tarawneh and Majdalaweyh [12] used sectional analysis with the Response-2000 software to investigate the load-carrying capacity of FRP-RC columns, achieving high accuracy (reliability index >3.5). Almomani et al. [11] employed Gene Expression Programming to develop predictive models for FRP-RC columns, accounting for eccentricity and slenderness. The P-Δ effect has also been addressed in several studies. Choo [5], Xue [13], and Hamid [7] all proposed analytical methods, with Xue modifying ACI 318-11's moment magnifier method, and Hamid implementing an iterative second-order analysis.

Although various analytical methods have been proposed to account for the contribution of compressive FRP reinforcement in evaluating the load-carrying capacity of eccentrically loaded FRP-RC columns, these approaches remain incomplete. Most existing methods focus primarily on failure modes governed by concrete crushing in the compression zone, without clearly distinguishing among different possible failure mechanisms. In addition, they often rely on simplified assumptions, such as employing an equivalent rectangular stress block for concrete, which can limit both their accuracy and practical applicability. To address this gap, this paper proposes an analytical method for evaluating the load-carrying capacity of eccentrically loaded FRP-RC columns, incorporating material constitutive laws and accounting for all theoretically potential failure modes. To achieve this, the following aspects are addressed:

(1) Classification of failure modes of FRP-RC columns under eccentric compression and development of corresponding strain and stress distribution across the cross-section for each failure mode
(2) Formulation of internal force equilibrium equations for each failure mode and construction of a computational flowchart
(3) Validation of the analytical model using experimental data from previous studies and comparison of the proposed method's accuracy with calculations based on ACI CODE-440.11.

The subsequent sections of the paper are organized as follows: Section 2 presents the analytical method for evaluating the load-carrying capacity of the column along with the computational flowchart; Section 3 discusses model validation; and Section 4 concludes the study and offers recommendations for future research on FRP-RC columns under eccentric loading.

2. Analytical Model Development

In this section, an analytical model is proposed to predict the load-carrying capacity of rectangular FRP-reinforced concrete columns under eccentric compression. The model incorporates strain compatibility, force equilibrium, and material constitutive laws to capture all potential failure modes and accounts for the compressive contribution of FRP rebars. Compared with conventional design methods, it provides more realistic and less conservative predictions.

2.1 Fundamental assumptions for calculations and constitutive laws of materials

Under eccentric compression, the column's cross-section is conventionally divided into two zones: the zone on the side of the applied force, which undergoes higher compressive stress, is referred to as the "compression zone"; the opposite zone, which experiences lower compressive stress or tension, is referred to as the "tension zone". The analytical method is developed based on the following assumptions: the plane section remains plane; the bond resistance between the concrete and FRP rebars

is constant; the strain compatibility and force equilibrium are satisfied; the maximum compressive strain of concrete (ε_{cu}) is 0.0035; the tensile resistance of concrete is ignored due to concrete's low tensile strength and the presence of cracks. Also, it should be emphasized that the present model is limited to short-term analysis of short FRP-RC columns under eccentric compression. It does not account for *P–Δ* effects, confinement effects, softening behavior of concrete, or time-dependent phenomena such as creep, shrinkage, and load duration.

To accurately assess the behavior of concrete, a simplified bilinear stress–strain relationship for compression, as defined in SP 63.13330.2018 [22], was adopted (Fig. 1 (a)). Meanwhile, a linear stress-strain relationship is used for FRP reinforcement under both compression and tension (Fig. 1 (b)). The contribution of FRP reinforcement in compression is considered in the calculations, with its compressive strength (f_{fcu}) defined as a fraction of its tensile strength (f_{fu}): $f_{fcu} = \beta_f f_{fu}$, where β_f is a coefficient representing the compressive-to-tensile strength ratio of the FRP rebar.

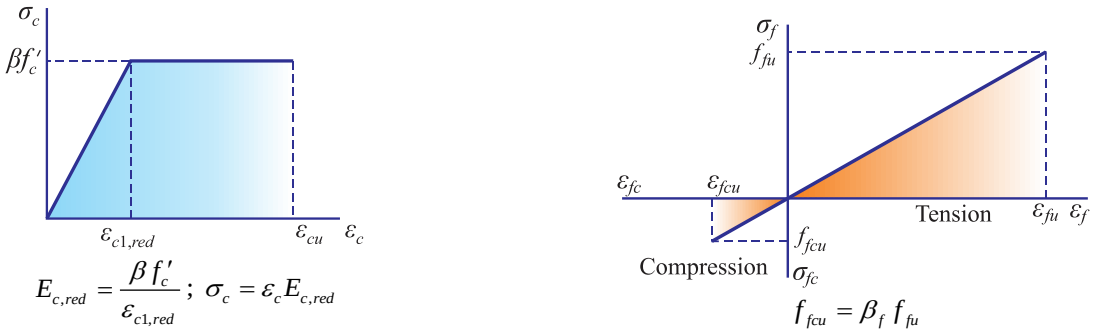

(a) Concrete (b) FRP rebar

Fig. 1 Constitutive laws of materials

2.2 *Analytical formulation for the balanced failure mode*

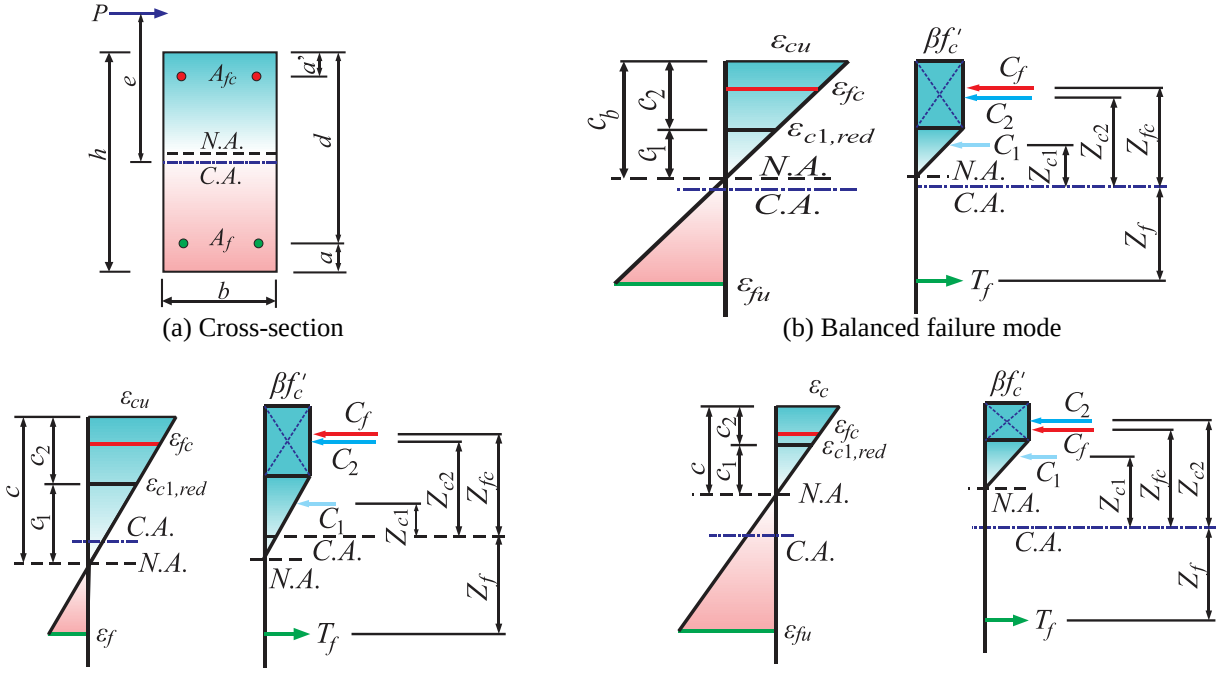

(a) Cross-section (b) Balanced failure mode

(c) Failure mode governed by concrete crushing (d) Failure mode governed by FRP rupture

Fig. 2 Cross-section geometry, strain, and stress distributions on the normal section for various failure modes

Studies have shown that the failure of eccentrically loaded FRP-RC columns can occur either in the tension zone - due to rupture of the FRP bars, or in the compression zone, where concrete crushing takes place while the FRP remains intact [5, 14, 21]. To distinguish between these two failure modes, a balanced failure condition is established. In this case, failure occurs simultaneously in both the tension and compression zones. Specifically, when the tensile strain in the FRP bars and the

compressive strain in the extreme concrete fiber both reach their ultimate limits at the same time. Fig. 2 illustrates the cross-section geometry, the corresponding strain and stress distributions for all possible failure modes, derived based on the material constitutive laws (Fig. 1) and the strain compatibility condition.

The height of the compression zone under balanced failure condition (c_b) is determined based on Fig. 2 (b) as

$$c_b = \frac{d\varepsilon_{cu}}{\varepsilon_{fu} + \varepsilon_{cu}} \tag{1}$$

where d is the effective depth, and ε_{fu} denotes the ultimate tensile strain of FRP rebar.

The resultant forces in the concrete compression zone C_1 and C_2 can be found by

$$C_1 = \frac{1}{2} b c_1 \beta f_c' \tag{2}$$

$$C_2 = b c_2 \beta f_c' \tag{3}$$

where b is the width of cross-section, β denotes the conversion factor from cylinder to prism compressive strength, and f'_c represents the cylinder compressive strength of concrete. In addition, c_1 and c_2 are the heights of the compressive concrete stress blocks, show in Fig. 2 (b), they can be computed by

$$c_1 = c_b \alpha \tag{4}$$

$$c_2 = c_b (1 - \alpha) \tag{5}$$

where α is the coefficient determined by

$$\alpha = \frac{1}{1 + \frac{\varepsilon_{cu} - \varepsilon_{c1,red}}{\varepsilon_{c1,red}}} \tag{6}$$

where $\varepsilon_{c1,red}$ is the limiting strain value at the transition between the elastic range and the horizontal plateau in the bilinear stress-strain diagram according to SP 63.13330.2018 [22], $\varepsilon_{c1,red}$ = 0.0015.

The strain (ε_{fc}) and the corresponding resultant force (C_f) in the FRP rebar located in the compression zone are calculated by

$$\varepsilon_{fc} = \frac{c_b - a'}{c_b} \varepsilon_{cu} \tag{7}$$

$$C_f = A_{fc} \beta_f \frac{c_b - a'}{c_b} \varepsilon_{cu} E_f \tag{8}$$

where A_{fc} and E_f denote the total area of FRP rebar in the concrete compression zone and its elastic modulus, respectively; a' is the distance from the centroid of the compressive reinforcement to the extreme compression face of the section.

The resultant force in tensile FRP rebar can be expressed as

$$T_f = f_{fu} A_f \tag{9}$$

where A_f denotes the total area of FRP rebar located in the concrete tension zone or in the less compressed region (in case of full-section compression).

The internal equilibrium of axial force and bending moment is expressed by Eqs. (10) - (11), respectively:

$$P_b = C_1 + C_2 + C_f - T_f \tag{10}$$

$$M_b = C_1 Z_{c1} + C_2 Z_{c2} + C_f Z_{fc} + T_f Z_f \tag{11}$$

where Z_{c1}, Z_{c2}, Z_{fc}, and Z_f represent the lever arms associated with the resultant forces C_1, C_2, C_f, and T_f, respectively (Fig. 2 (b)). When calculating moments about an axis that passes through the centroid axis and is perpendicular to the bending plane, these values are calculated as

$$Z_{c1} = \frac{h}{2} - \frac{c_1}{3} - c_2 \tag{12}$$

$$Z_{c2} = 0.5\left(h - c_2\right) \tag{13}$$

$$Z_{fc} = \frac{h}{2} - a' \tag{14}$$

$$Z_f = \frac{h}{2} - a \tag{15}$$

The eccentricity of the axial force in the case of balanced failure is determined by

$$e_b = \frac{M_b}{P_b} \tag{16}$$

Based on the compression zone height or eccentricity at the balanced failure condition, the failure mode of the column is classified as follows: if $c \geq c_b$ or $e_{exp} \leq e_b$, failure initiates in the concrete compression zone; conversely, if $c < c_b$ or $e_{exp} > e_b$, the column fails due to rupture of the tensile FRP reinforcement, where e is the eccentricity induced by external loading.

2.3 Analytical formulation for the failure mode governed by concrete crushing

The concrete crushing failure mode in the compression zone is the predominant failure mode for FRP-RC columns subjected to eccentric compression. This failure mode is observed in nearly all experimental research results. Failure occurs when the compressive strain in concrete (on the loaded edge) reaches its ultimate value ε_{cu} (Fig. 2 (c)). The tensile (ε_f) and compressive strains (ε_{fc}) in FRP rebars are determined by

$$\varepsilon_f = \frac{d - c}{c} \varepsilon_{cu} \leq \varepsilon_{fu} \tag{17}$$

$$\varepsilon_{fc} = \varepsilon_{cu} \frac{c - a'}{c} \leq \varepsilon_{fcu} \tag{18}$$

where c represents the depth of the compression zone of the cross-section, and ε_{fcu} denotes the ultimate compressive strain of FRP rebars.

The resultant tensile force (T_f) and compressive force (C_f) in the FRP reinforcement are determined by

$$T_f = E_f A_f \frac{d - c}{c} \varepsilon_{cu} \tag{19}$$

$$C_f = E_f A_f \beta_f \frac{c - a'}{c} \varepsilon_{cu} \tag{20}$$

The resultant force in the concrete compression zones C_1 and C_2 can be found by

$$C_1 = \frac{1}{2} b c_1 \beta f_c' \tag{21}$$

$$C_2 = b c_2 \beta f_c' \tag{22}$$

where c_1 and c_2 are the heights of the compressive concrete stress blocks, as shown in Fig. 2 (c), and can be computed by

$$c_1 = c\alpha \tag{23}$$

$$c_2 = c(1 - \alpha) \tag{24}$$

The internal equilibrium of axial force and bending moment is expressed, respectively, by

$$P = C_1 + C_2 + C_f - T_f \tag{25}$$

$$M = C_1 Z_{c1} + C_2 Z_{c2} + C_f Z_{fc} + T_f Z_f \tag{26}$$

where the lever arms Z_{c1}, Z_{c2}, Z_{fc}, and Z_f are determined by Eqs. (12) - (15).

The eccentricity of the axial force is determined by

$$e = \frac{M}{P} \tag{27}$$

2.4. Analytical formulation for the failure mode governed by FRP rupture

In the case of failure due to FRP rupture, the tensile strain in the FRP reinforcement reaches its ultimate limit. Based on the strain distribution diagram for this failure mode (Fig. 2 (d)), the strain values in the materials are determined with respect to the depth of the compression zone.

The strain and resultant force in the FRP rebar located in the compression zone can be determined by

$$\varepsilon_{fc} = \frac{(c - a')\varepsilon_{fu}}{d - c} \tag{28}$$

$$C_f = \varepsilon_{fc} \beta_f E_f A_f \tag{29}$$

The resultant force in FRP rebar located in the tension zone can be computed by

$$T_f = f_{fu} A_f \tag{30}$$

Maximum strain in the outermost compressed concrete fiber can be found by

$$\varepsilon_c = \frac{c\varepsilon_{fu}}{d - c} \tag{31}$$

The resultant force in the compressed concrete area is determined based on the strain in the outermost compressed fiber. When $\varepsilon_c > \varepsilon_{c1,red}$, the stress distribution in the concrete compression zone is split into two regions, as illustrated in Fig. 2 (d). Accordingly, the heights c_1 and c_2 of these zones, along with their respective resultant forces C_1 and C_2, are calculated by

$$c_1 = \frac{\varepsilon_{c1,red}}{\varepsilon_{fu}}(d - c) \tag{32}$$

$$c_2 = c - c_1 \tag{33}$$

$$C_1 = \frac{1}{2} b c_1 \beta f_c' \tag{34}$$

$$C_2 = \beta f_c' b c_2 \tag{35}$$

The load-carrying capacity of the column is determined using the axial force and moment equilibrium Eqs. (25) - (26), with the lever arms in Eq. (26) calculated based on Eqs. (12) - (15).

When $\varepsilon_c \leq \varepsilon_{c1,red}$, due to the small compressive strain in the concrete, the stress in the compression zone follows a triangular distribution. As a result, resultant force C_2 equals zero, and C_1 is calculated by

$$C_1 = \frac{1}{2} b c \varepsilon_c E_{cred} \tag{36}$$

where $E_{c,red}$ denotes the reduced deformation modulus of compressive concrete.

The internal equilibriums of axial force and bending moment are expressed by Eqs. (25) - (26), respectively. The lever arms Z_{fc} and Z_f in Eq. (26) are calculated based on Eqs. (14) - (15), while the lever arm Z_{c1} is calculated by

$$Z_{c1} = \frac{h}{2} - \frac{c}{3} \tag{37}$$

The eccentricity of the axial force for this failure mode is determined in the same manner as for the failure mode governed by concrete crushing, that is, according to Eq. (27).

2.5. Calculation flowchart

The theoretical load-carrying capacity of an eccentrically loaded FRP-RC column is determined through the following procedure: First, the failure mode is identified based on the comparison between the balanced eccentricity (e_b) and the applied eccentricity (e_{exp}). Next, an iterative calculation process is carried out: for each assumed value of the compression zone height (c), the corresponding force components (C_1, C_2, C_f, and T_f) and their respective lever arms (Z_{c1}, Z_{c2}, Z_{fc}, and Z_f) are calculated. These values are then used to determine the axial force (P), bending moment (M), and theoretical eccentricity (e). The iteration continues until the theoretical eccentricity (e) closely matches the experimental eccentricity. At this point, the corresponding P and M values represent the theoretical load-carrying capacity of the column. The calculation flowchart is illustrated in Fig. 3.

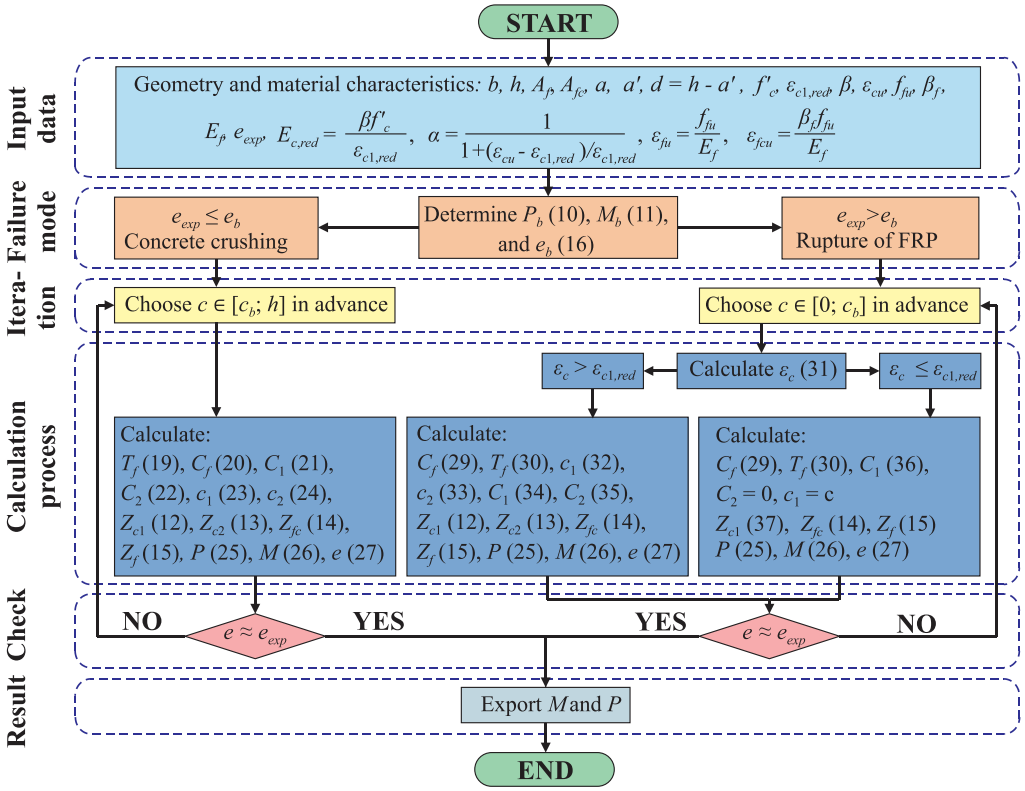

Fig. 3 Flowchart for calculating the load-carrying capacity of FRP-RC columns under eccentric loading

3. Model Validation

To validate the proposed model, a dataset of 91 rectangular-section FRP-RC columns subjected to eccentric axial compression was compiled from 16 different sources [1, 4, 6-9, 14, 16, 23-30]. These experimental specimens were sourced from reputable peer-reviewed journals published between 2003 and 2024. A summary of the key parameters is presented in Table 1, with complete descriptions provided in the Appendix. The dataset exhibits a wide variation in geometry, material properties, and loading conditions, enabling comprehensive validation across different structural configurations.

Column dimensions (length: 780 - 2000 mm; width and height: 150 - 405 mm) indicate a broad range of slenderness ratios (λ = 13.23 - 39.35), which significantly influence stability under eccentric loading. The reinforcement types include GFRP, CFRP, and BFRP, with total reinforcement ratios (ρ_{ft}) ranging from 0.38% to 3.88%. These variations affect the stiffness and ductility of the columns. The eccentricity ratio (e/h = 0.096 - 1.0) captures a spectrum from nearly concentric to highly eccentric loading. The concrete compressive strength (f'_c = 27.73 - 47.3 *MPa*) spans from normal-strength to moderately

high-strength concrete, affecting confinement behavior and strain compatibility, especially in failure modes involving concrete crushing or FRP bar instability. The wide-ranging properties presented in the dataset not only validate the model's robustness but also provide insights into how geometric and material parameters influence column behavior under eccentric axial compression.

Table 1 Summary of experimental parameters of the tested columns collected from previous studies

Year	*l*, *mm*	*b*, *mm*	*h*, *mm*	λ	Rebar	ρ_{ft}, %	f_{fu}, *MPa*	E_f, *GPa*	*e/h*	f'_c, *MPa*
2003-2025	780-2000	150-405	150-405	13.23-39.35	GFRP CFRP BFRP	0.38-3.88	347.5-2550	32.67-151	0.096-1.0	27.73-47.3

As previously mentioned, the ratio of compressive to tensile strength of FRP reinforcement varies over a wide range. Therefore, to verify the model, a conservative reduction factor of β_f = 0.3 is adopted, in line with recommendations from previous studies [3]. Additionally, the compressive strength of cubic concrete samples was converted to cylindrical sample strength using a factor of 0.893.

Beyond being verified against experimental data, the proposed model was also compared with theoretical outcomes derived from the ACI CODE-440.11 [18] (P_{ACI}, $P_{ACI,nor}$), which neglects the compressive contribution of FRP reinforcement. The Appendix details the load-carrying capacity of the experimental columns as predicted by both the proposed method and ACI CODE-440.11. Fig. 4 compares the normalized load-carrying capacities predicted by the proposed model and those calculated using the ACI CODE-440.11 standard. The proposed model shows slightly better alignment with experimental data.

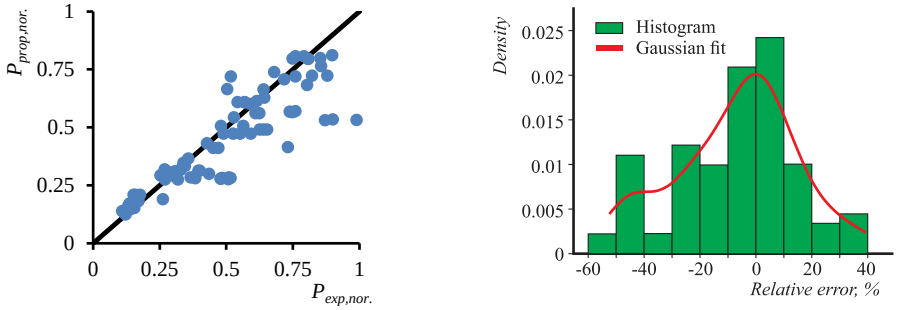

(a) Proposed model

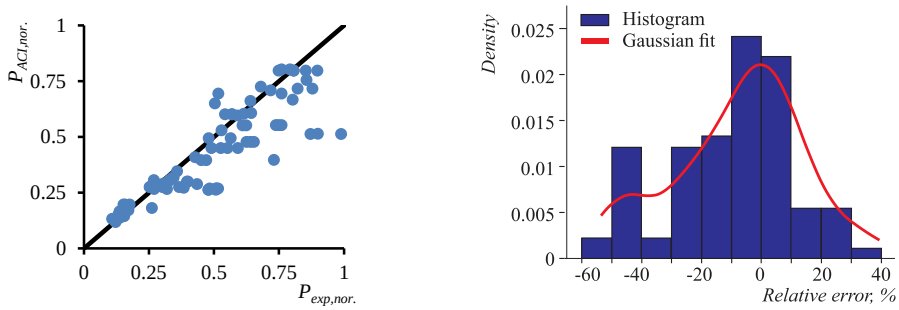

(b) ACI CODE-440.11

Fig. 4 Comparison between theoretical and experimental normalized load-carrying capacity, and possible error distribution histograms

The statistical comparison in Table 2 demonstrates that the proposed method provides improved accuracy over ACI CODE-440.11 in predicting the behavior of FRP-RC columns under eccentric compression. Specifically, the proposed model yields a mean value of 0.932, closer to the experimental results than the ACI CODE-440.11's 0.896. Its Pearson correlation coefficient (*r*) of 0.84 also slightly exceeds the ACI's 0.83, indicating enhanced consistency in predictions. While the coefficient of variation (COV) and standard deviation (SD) are comparable between the two approaches, the proposed model shows a modest but meaningful improvement in estimating the load-carrying capacity. It is also worth noting that a compressive strength reduction factor of β_f = 0.3 was adopted in the verification process, representing a conservative

assumption. In practice, the compressive strength of FRP bars may be higher; therefore, the accuracy of the proposed model could further improve and align more closely with the experimental results. Overall, the proposed method offers a more accurate and reliable alternative for the design of FRP-RC columns subjected to eccentric loading.

Table 2 Statistical comparison of theoretical against experimental results

Method	$P_{prop.nor}/P_{exp.nor}$	RMSE	COV, %	SD	r
Proposed	0.932	0.154	22.9	0.145	0.84
ACI CODE-440.11	0.896	0.161	22.7	0.148	0.83

In addition to the comparative statistical metrics mentioned earlier, the reliability of the computational method is further assessed through the ratio $P_{prop.nor}/P_{exp.nor}$ for key parameters affecting the load-carrying capacity of eccentrically compressed FRP-RC columns. These parameters include concrete strength, slenderness ratio, eccentricity ratio e/h, elastic modulus of FRP rebar, strength of FRP rebar, and reinforcement ratio as shown in Fig. 5. From Fig. 5, it is evident that the predictions yield a nearly flat trend for all variables except the reinforcement ratio (Fig. 5 (f)). In this case, the negative slope indicates an underestimation of the load-carrying capacity.

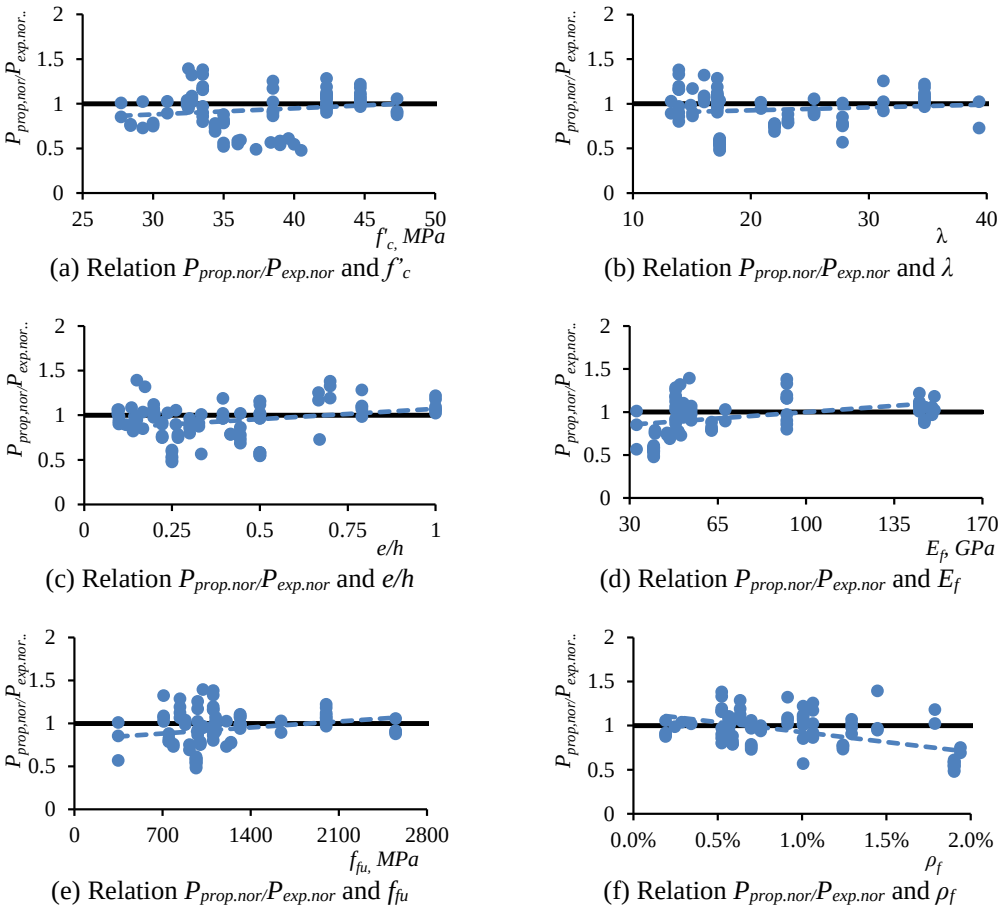

(a) Relation $P_{prop.nor}/P_{exp.nor}$ and f'_c (b) Relation $P_{prop.nor}/P_{exp.nor}$ and λ

(c) Relation $P_{prop.nor}/P_{exp.nor}$ and e/h (d) Relation $P_{prop.nor}/P_{exp.nor}$ and E_f

(e) Relation $P_{prop.nor}/P_{exp.nor}$ and f_{fu} (f) Relation $P_{prop.nor}/P_{exp.nor}$ and ρ_f

Fig. 5 Accuracy of the proposed analytical model in predicting the behavior of FRP-RC columns, under eccentric loading for various structural parameters

To assess the contribution of FRP reinforcement to the axial compressive capacity, the relationship between the ratio C_f/P_{prop} and the compressive reinforcement ratio ρ_{fc} is constructed and shown in Fig. 6. It is evident from Fig. 6 that the contribution of FRP bars to the column's load-carrying capacity is substantial and increases progressively with higher reinforcement ratios. Based on the results of 91 tested columns, the contribution of compressive FRP reinforcement ranges from 0.94% to 22.28%, with an average value of 4.25%, corresponding to a variation in ρ_{fc} from 0.19% to 1.94%. However, it should be noted that the contribution of FRP reinforcement to axial capacity is not solely governed by the compressive reinforcement ratio, but also significantly influenced by other parameters, such as load eccentricity, tie spacing, material

properties, and cross-sectional geometry.

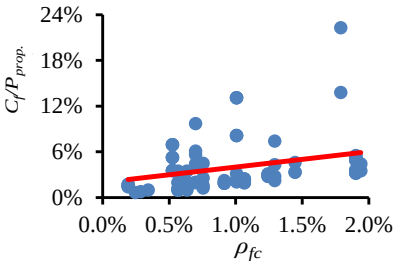

Fig. 6 Contribution of compressive FRP reinforcement

Additionally, the current experimental data on eccentrically loaded FRP-RC columns remain limited in both the number of specimens and the range of test parameters, particularly the degree of eccentricity. Among the 91 specimens compiled from prior studies (see Appendix), eccentricity values range only from 0.096 to 1.0, with no instances of high eccentricity. As a result, failure in these specimens is typically due to concrete crushing in the compression zone, while the FRP reinforcement in the tension zone generally remains intact. Therefore, the analytical model proposed in this study has not been validated for failure modes involving FRP rupture, highlighting a significant research gap. This issue is intended to be addressed in future studies through both experimental testing and numerical simulations.

Furthermore, the proposed model does not yet account for key factors affecting column load-carrying capacity, such as longitudinal bending, the role of transverse reinforcement, or random eccentricity. Consequently, discrepancies persist between the theoretical load-carrying capacity predicted by the model and experimental results, which are not yet fully satisfactory. Addressing these challenges will be a primary objective of future research.

4. Conclusions

This study developed an analytical model to predict the load-carrying capacity of rectangular FRP-RC columns under eccentric compression. The proposed model is established based on strain compatibility and force equilibrium conditions. It incorporates the specific stress-strain relationships of both concrete and FRP reinforcement and also considers the contribution of compressive FRP rebars to the overall sectional capacity. The model was validated using a database of 91 experimentally tested columns collected from reputable publications. The main findings can be summarized as follows:

(1) Two primary failure modes of FRP-RC columns under eccentric compression were identified: concrete crushing and FRP rupture, separated by a balanced failure condition.

(2) An analytical approach and a corresponding computational framework were established to estimate the load-carrying capacity across all possible failure modes of FRP-RC columns under eccentric loading.

(3) The proposed model demonstrated high predictive accuracy, with a mean predicted-to-experimental strength ratio of 0.932, RMSE = 0.154, COV = 22.9%, SD = 0.145, and correlation coefficient r = 0.84, outperforming ACI CODE-440.11 in most cases.

(4) The contribution of compressive FRP reinforcement was found to be significant, enhancing column strength by 0.94% to 22.3%, depending on reinforcement ratio and eccentricity. This finding highlights the importance of including the contribution of compressive FRP rebars in design formulations rather than neglecting them for conservative design.

Despite its promising performance, the model remains limited in scope. It does not account for P–Δ effects, confinement from transverse reinforcement, or time-dependent behavior. Furthermore, the current dataset lacks sufficient high-eccentricity columns to validate failure modes governed by FRP rupture. Future research should address these limitations and explore the influence of longitudinal bending and multi-layer FRP reinforcement. These advancements would broaden the applicability ò the model and support its integration into design codes.

Conflicts of Interest

The authors declare no conflict of interest.

Notation

a	Distance from the centroid of the tensile reinforcement (A_f) to the outermost tension fiber of the cross-section
a'	Distance from the centroid of the compressive reinforcement (A_{fc}) to the extreme compression face of the section
A_f	Total area of FRP rebar located in the concrete tension zone or in the less compressed region (in case of full-section compression)
A_{fc}	Total area of FRP rebar in the concrete compression zone
b	Width of the cross-section of the column
c	Depth of the compression zone of the cross-section
c_b	Depth of the compression zone of the cross-section at the balanced failure
c_1	Depth of the rectangular stress block in the concrete compression zone
C_1	Resultant compressive force in the concrete compression zone with uniformly distributed stress
c_2	Depth of the triangular stress block in the concrete compression zone
C_2	Resultant compressive force in the concrete compression zone with triangularly distributed stress
C_f	Resultant internal force in FRP rebar in the concrete compression zone
d	Effective depth of the cross-section of the column
e	Eccentricity of the axial force
$E_{c,\,red}$	Reduced the deformation modulus of compressive concrete
e_{exp}	Experimental eccentricity of the axial force
e_b	Theoretical eccentricity of the axial force at balanced failure mode
E_f	Elastic modulus of FRP rebar
f'_c	Cylinder compressive strength of concrete
f_{fcu}	Ultimate compressive strength of FRP rebar
f_{fu}	Ultimate tensile strength of FRP rebar
h	Height of the cross-section of the column
l	Total length of the tested column
M	Bending moment
C.A.	Centroid axis
N.A.	Neutral axis
P	Axial force
P_{exp}	Experimental axial force
$P_{exp.\,nor}$	Normalized experimental axial force - $P_{exp.nor} = P_{exp}/(0.85f'_cA_g)$
P_{prop}	Axial force obtained from the proposed analytical method
$P_{prop.nor}$	Normalized axial force obtained from the proposed analytical method - $P_{prop.nor} = P_{prop}/(0.85f'_cA_g)$
P_{ACI}	Axial force calculated according to the ACI CODE-440.11-22
$P_{ACI.nor}$	Normalized axial force calculated according to the ACI CODE-440.11-22
T_f	Resultant internal force in FRP rebar located in the concrete tension zone or in the less compressed region (in case of full-section compression)
Z_{c1}	Lever arm of the compressive force C_1, i.e., the distance from the line of action of C_1 to the centroid axis
Z_{c2}	Lever arm of the compressive force C_2, i.e., the distance from the line of action of C_2 to the centroid axis
Z_f	Lever arm of the tensile force T_f, i.e., the distance from the line of action of T_f to the centroid axis
Z_{fc}	Lever arm of the compressive force C_f, i.e., the distance from the line of action of C_f to the centroid axis
α	Coefficient $\alpha = \dfrac{1}{1+\left(\varepsilon_{cu}-\varepsilon_{c1red}\right)/\varepsilon_{c1red}}$
β	Conversion factor from cylinder to prism compressive strength
β_f	Conversion factor for translating FRP tensile strength to its equivalent compressive strength
ε_c	Compressive strain in concrete
$\varepsilon_{c1,red}$	Limiting strain value at the transition between the elastic range and the horizontal plateau in the bilinear reduced stress-strain diagram according to SP 63.13330.2018, $\varepsilon_{c1,\,red} = 0.0015$
ε_{cu}	Ultimate compressive strain of concrete
ε_f	Tensile strain in FRP rebar
ε_{fc}	Compressive strain in FRP rebar
ε_{fcu}	Ultimate compressive strain of FRP rebar
ε_{fu}	Ultimate tensile strain of FRP rebar
λ	Slenderness ratio of the column
σ_c	Compressive stress in concrete
ρ_f	Tensile reinforcement ratio
ρ_{fc}	Compressive reinforcement ratio

ρ_{ft} Total reinforcement ratio, $\rho_{ft} = \rho_f + \rho_{fc}$

References

[1] M. K. Sharbatdar, "Concrete Columns and Beams Reinforced with FRP Bars and Grids under Monotonic and Reversed Cyclic Loading," Ph.D. dissertation, Department of Civil Engineering, University of Ottawa, Ottawa, 2003.

[2] H. Dang Vu and D. N. Phan, "Experimental and Theoretical Analysis of Cracking Moment of Concrete Beams Reinforced with Hybrid Fiber Reinforced Polymer and Steel Rebars," Advances In Technology Innovation, vol. 6, no. 4, pp. 222-234, 2021.

[3] K. Khorramian and P. Sadeghian, "Material Characterization of GFRP Bars in Compression Using a New Test Method," Journal of Testing and Evaluation, vol. 49, no. 2, pp. 1037-1052, 2021.

[4] N. Elmesalami, F. Abed, and A. E. Refai, "Concrete Columns Reinforced with GFRP and BFRP Bars under Concentric and Eccentric Loads: Experimental Testing and Analytical Investigation," Journal of Composites for Construction, vol. 25, no. 2, article no. 04021003, 2021.

[5] C. C. Choo, I. E. Harik, and H. Gesund, "Strength of Rectangular Concrete Columns Reinforced with Fiber-Reinforced Polymer Bars," ACI Structural Journal, vol. 103, no. 3, pp. 452-459, 2006.

[6] L. Sun, M. Wei, and N. Zhang, "Experimental Study on the Behavior of GFRP Reinforced Concrete Columns under Eccentric Axial Load," Journal of Composites for Construction, vol. 152, pp. 214-225, 2017.

[7] F. L. Hamid and A. R. Yousif, "Behavior of Short and Slender RC Columns with BFRP Bars under Axial and Flexural Loads: Experimental and Analytical Investigation," Journal of Composites for Construction, vol. 28, no. 1, article no. 4465, 2023.

[8] M. Guérin, H. M. Mohamed, B. Benmokrane, A. Nanni, and C. K. Shield, "Eccentric Behavior of Full-Scale Reinforced Concrete Columns with Glass Fiber-Reinforced Polymer Bars and Ties," Structural Journal, vol. 115, no. 2, pp. 489-499, 2018.

[9] M. Guérin, H. M. Mohamed, B. Benmokrane, C. K. Shield, and A. Nanni, "Effect of Glass Fiber-Reinforced Polymer Reinforcement Ratio on Axial-Flexural Strength of Reinforced Concrete Columns," Structural Journal, vol. 115, no. 4, pp. 1049-1061, 2018.

[10] A. S. Hosseini and P. Sadeghian, "Assessing Compressive Properties of GFRP Bars: Novel Test Fixture and Statistical Analysis," Journal of Composites for Construction, vol. 29, no. 2, p. 04025011, 2025.

[11] Y. Almomani, A. Tarawneh, R. Alawadi, Z. N. Taqieddin, Y. Jweihan, and E. Saleh, "Predictive Models of Behavior and Capacity of FRP Reinforced Concrete Columns," Journal of Applied Engineering Science, vol. 21, no. 1, pp. 143-156, 2023.

[12] A. Tarawneh and S. Majdalaweyh, "Design and Reliability Analysis of FRP-Reinforced Concrete Columns," Structures, vol. 28, pp. 1580-1588, 2020.

[13] W. Xue, F. Peng, and Z. Fang, "Behavior and Design of Slender Rectangular Concrete Columns Longitudinally Reinforced with Fiber-Reinforced Polymer Bars," ACI Structural Journal, vol. 115, no. 2, pp. 311-322, 2018.

[14] M. Elchalakani and G. Ma, "Tests of Glass Fibre Reinforced Polymer Rectangular Concrete Columns Subjected to Concentric and Eccentric Axial Loading," Engineering Structures, vol. 151, pp. 93-104, 2017.

[15] M. Elchalakani, G. Ma, F. Aslani, and W. Duan, "Design of GFRP-Reinforced Rectangular Concrete Columns under Eccentric Axial Loading," Magazine of Concrete Research, vol. 69, no. 17, pp. 865-877, 2017.

[16] Z. S. Othman and A. H. Mohammad, "Behaviour of Eccentric Concrete Columns Reinforced with Carbon Fibre-Reinforced Polymer Bars," Advances in Civil Engineering, vol. 2019, no. 1, article no. 1769212, 2019.

[17] ACI Committee 440, "Guide for the Design and Construction of Structural Concrete Reinforced with FRP Bars," ACI, Farmington Hills, MI, USA, Rep. 440.1R-15, 2015.

[18] Building Code Requirements for Structural Concrete Reinforced with Glass Fiber Reinforced Polymer (GFRP) Bars - Code and Commentary, ACI CODE-440.11-22, 2023.

[19] Design and Construction of Building Structures with Fibre-Reinforced Polymers, CSA S806:2012:R2017, 2017.

[20] Concrete Structures Reinforced with Fibre-Reinforced Polymer Bars. Design Rules, SP 295.1325800.2017, 2017

[21] H. J. Zadeh and A. Nanni, "Design of RC Columns Using Glass FRP Reinforcement," Journal of Composites for Construction, vol. 17, no. 3, pp. 294-304, 2013.

[22] Concrete and Reinforced Concrete Structures. General Provisions, SP 63.13330.2018, 2019.

[23] M. Issa, I. Metwally, and S. Elzeiny, "Performance of Eccentrically Loaded GFRP Reinforced Concrete Columns," World Journal of Engineerning, vol. 9, no. 1, pp. 71-78, 2012.

[24] M. N. S. Hadi and J. Youssef, "Experimental Investigation of GFRP-Reinforced and GFRP-Encased Square Concrete Specimens under Axial and Eccentric Load, and Four-Point Bending Test," Journal of Composites for Construction, vol. 20, no. 5, article no. 04016020, 2016.

[25] A. K. Pour, A. Shirkhani, M. S. Kırgız, and E. N. Farsangi, "Experimental Investigation of GFRP-Reinforced Concrete Columns Made with Waste Aggregates under Concentric and Eccentric Loads," Structural Concrete, vol. 24, no. 1, pp. 1670-1688, 2022

[26] M. S. Irhayyim, W. A. Aules, and M. M. Jomaa'h, "Structural Behavior of Reinforced Concrete Columns Fully and Partially Reinforced with GFRP Bars Tested under Concentric or Eccentric Compressive Loads," Diyala Journal of Engineering Sciences, vol. 17, no. 3, pp. 58–77, 2024.

[27] H. G. Fathi, M. K. N. Ghali, A. S. Shanour, and A. N. M. Khater, "Experimental and Analytical Study on Eccentrically Loaded Fiber Concrete Columns Reinforced Longitudinally with GFRP Bars," Engineering Structures, vol. 312, article no. 118251, 2024.
[28] N. S. Mahmoudabadi, A. Bahrami, S. Saghir, A. Ahmad, M. Iqbal, M. Elchalakani, and Y. O. Özkılıç, "Effects of Eccentric Loading on Performance of Concrete Columns Reinforced with Glass Fiber-Reinforced Polymer Bars," Scientific Reports, vol. 14, no. 1, article no. 1890, 2024.
[29] A. S. Hosseini and P. Sadeghian, "Slenderness Effect on GFRP-RC Columns with Square Spirals under Concentric and Eccentric Loading: Experimental and Analytical Study," Engineering Structures, vol. 334, article no. 120277, 2025.
[30] S. A. Emam, O. Amer, A. H. Ali, and H. A. Haggag, "Experimental Investigation on the Compressive Behaviour of GFRP-Reinforced Concrete Short Columns," Engineering Research Journal, vol. 184, no. 3, pp. 44-58, 2025.

Appendix

Table A1 Database of tested eccentrically loaded FRP-RC columns

Ref.	*Specimen's ID*	*Geometry*						*Main reinforcement*					*Concrete*	*Test results*		*Proposed*		*ACI CODE-440.11*	
		l, mm	*b, mm*	*h, mm*	*d, mm*	*λ*	*e/h*	*FRP type*	*A_f, mm^2*	*ρ_{ft}, %*	*f_{fu}, MPa*	*E_f, GPa*	*f'c, MPa*	*P_{exp}, kN*	*$P_{exp.nor}$*	*P_{prop}*	*$P_{prop.nor}$*	*P_{ACI}*	*$P_{ACI.nor}$*
Sharbatdar [1]	CFS1	1680	230	230	226	25.4	0.26	CFRP	100.6	0.38	2550	147	47.3	1020	0.48	1077.6	0.51	1053	0.5
	CFS2	1680	230	230	226	25.4	0.33	CFRP	100.6	0.38	2550	147	47.3	1000	0.47	875.6	0.41	841.2	0.4
	CFS3	1680	230	230	226	25.4	0.26	CFRP	100.6	0.38	2550	147	47.3	1200	0.564	1077.6	0.51	1053	0.5
	CFS4	1680	230	230	226	25.4	0.33	CFRP	100.6	0.38	2550	147	47.3	960	0.451	875.6	0.41	841.2	0.4
Issa, et al. [23]	GN8	1200	150	150	144	27.8	0.33	GFRP	226.2	2.01	347.5	32.67	27.7	227.1	0.428	228.9	0.43	217.4	0.41
	GN13	1200	150	150	144	27.8	0.17	GFRP	226.2	2.01	347.5	32.67	27.7	425.8	0.803	362.6	0.68	353.6	0.67
	GM8	1200	150	150	144	27.8	0.33	GFRP	226.2	2.01	347.5	32.67	38.4	535.8	0.731	304.7	0.41	291.3	0.4
Hadi and Youssef [24]	RF-25	800	210	210	177	13.2	0.12	GFRP	253.4	1.15	1641	67.9	31	995	0.856	888.6	0.76	879	0.76
	RF-50	800	210	210	177	13.2	0.24	GFRP	253.4	1.15	1641	67.9	31	615	0.529	632.5	0.54	615.9	0.53
Elchalakani and Ma [14]	G150-25	1200	160	260	228	16	0.1	GFRP	380.1	1.83	708	50	32.75	880.3	0.76	935.4	0.81	930	0.8
	G150-45	1200	160	260	228	16	0.17	GFRP	380.1	1.83	708	50	32.75	584.2	0.504	771.7	0.67	753.8	0.65
	G75-25	1200	160	260	228	16	0.1	GFRP	380.1	1.83	708	50	32.75	917.2	0.792	935.4	0.81	930	0.8
	G75-35	1200	160	260	228	16	0.14	GFRP	380.1	1.83	708	50	32.75	787.8	0.68	856.2	0.74	841.1	0.73
Sun, et al. [6]	Z175-1	1000	180	250	225	13.9	0.7	GFRP	235.5	1.05	1103	92.4	29.9	201	0.176	240.7	0.21	225	0.2
	Z175-2	1000	180	250	225	13.9	0.7	GFRP	235.5	1.05	1103	92.4	29.9	174	0.152	240.7	0.21	225	0.2
	Z175-3	1000	180	250	225	13.9	0.7	GFRP	235.5	1.05	1103	92.4	29.9	181	0.158	240.7	0.21	225	0.2
	Z125-1	1000	180	250	225	13.9	0.5	GFRP	235.5	1.05	1103	92.4	29.9	291	0.254	336.6	0.29	316	0.28
	Z125-2	1000	180	250	225	13.9	0.5	GFRP	235.5	1.05	1103	92.4	29.9	290	0.253	336.6	0.29	316	0.28
	Z125-3	1000	180	250	225	13.9	0.5	GFRP	235.5	1.05	1103	92.4	29.9	347	0.303	336.6	0.29	316	0.28
	Z75-1	1000	180	250	225	13.9	0.3	GFRP	235.5	1.05	1103	92.4	29.9	632	0.552	542.1	0.47	516.7	0.45
	Z75-2	1000	180	250	225	13.9	0.3	GFRP	235.5	1.05	1103	92.4	29.9	677	0.592	542.1	0.47	516.7	0.45
	Z75-3	1000	180	250	225	13.9	0.3	GFRP	235.5	1.05	1103	92.4	29.9	602	0.526	542.1	0.47	516.7	0.45
Guérin, et al. [8]	CGA40	2000	405	405	357	17.2	0.1	GFRP	927	1.13	1317	51.3	42.3	4760	0.807	4696.2	0.80	4705.8	0.8
	CGA80	2000	405	405	357	17.2	0.2	GFRP	927	1.13	1317	51.3	42.3	3354	0.569	3593.1	0.61	3551.3	0.6
	CGA160	2000	405	405	357	17.2	0.4	GFRP	927	1.13	1317	51.3	42.3	1943	0.329	1875.5	0.32	1797.5	0.31
	CGA320	2000	405	405	357	17.2	0.79	GFRP	927	1.13	1317	51.3	42.3	745	0.126	813.3	0.14	769.8	0.13
	CGB40	2000	405	405	357	17.2	0.1	GFRP	1038	1.27	838	48.2	42.3	4417	0.749	4699.6	0.80	4706.2	0.8
	CGB80	2000	405	405	357	17.2	0.2	GFRP	1038	1.27	838	48.2	42.3	3200	0.543	3596.4	0.61	3552.2	0.6
	CGB160	2000	405	405	357	17.2	0.4	GFRP	1038	1.27	838	48.2	42.3	1589	0.269	1890.1	0.32	1810.1	0.31
	CGB320	2000	405	405	357	17.2	0.79	GFRP	1038	1.27	838	48.2	42.3	645	0.109	826.6	0.14	783.8	0.13
M. Guérin, et al. [9]	G1e10	2000	405	405	360	17.2	0.1	GFRP	927	1.13	1317	51.3	42.3	4760	0.807	4695.5	0.80	4707.3	0.8
	G1e20	2000	405	405	360	17.2	0.2	GFRP	927	1.13	1317	51.3	42.3	3357	0.569	3595.7	0.61	3552.6	0.6
	G1e40	2000	405	405	360	17.2	0.4	GFRP	927	1.13	1317	51.3	42.3	1942	0.329	1883.3	0.32	1803.8	0.31
	G1e80	2000	405	405	360	17.2	0.79	GFRP	927	1.13	1317	51.3	42.3	745	0.126	820.7	0.14	774.9	0.13
	G2e10	2000	405	405	360	17.2	0.1	GFRP	1236	1.51	1317	51.3	42.3	5028	0.853	4716.5	0.80	4707.3	0.8
	G2e20	2000	405	405	360	17.2	0.2	GFRP	1236	1.51	1317	51.3	42.3	3625	0.615	3623.8	0.61	3562.3	0.6
	G2e40	2000	405	405	360	17.2	0.4	GFRP	1236	1.51	1317	51.3	42.3	2035	0.345	1969.3	0.33	1881.7	0.32
	G2e80	2000	405	405	360	17.2	0.79	GFRP	1236	1.51	1317	51.3	42.3	914	0.155	903	0.15	853.2	0.15
	G3e10	2000	405	405	357	17.2	0.1	GFRP	2120	2.58	1122	54.4	42.3	5294	0.898	4787	0.81	4704.5	0.8
	G3e20	2000	405	405	357	17.2	0.2	GFRP	2120	2.58	1122	54.4	42.3	3790	0.643	3707.3	0.63	3585.5	0.61
	G3e40	2000	405	405	357	17.2	0.4	GFRP	2120	2.58	1122	54.4	42.3	2110	0.358	2157.6	0.37	2042.7	0.35
	G3e80	2000	405	405	357	17.2	0.79	GFRP	2120	2.58	1122	54.4	42.3	1008	0.171	1081.8	0.18	1012.5	0.17
Othman and Mohammad [16]	C10-T90-E0.5	1500	150	150	124	34.7	0.5	CFRP	157	1.4	2000	150	44.7	258	0.302	249.8	0.29	236.8	0.28
	C10-T90-E1.0	1500	150	150	124	34.7	1	CFRP	157	1.4	2000	150	44.7	119	0.139	125.9	0.15	119	0.14
	C12-T90-E0.5	1500	150	150	123	34.7	0.5	CFRP	226.2	2.01	2000	145	44.7	262	0.306	265.5	0.31	249.1	0.29
	C12-T90-E1.0	1500	150	150	123	34.7	1	CFRP	226.2	2.01	2000	145	44.7	126	0.147	137.6	0.16	129.5	0.15
	C16-T90-E0.5	1500	150	150	121	34.7	0.5	CFRP	402.2	3.58	2000	151	44.7	290	0.339	296.8	0.35	268.9	0.32
	C16-T90-E1.0	1500	150	150	121	34.7	1	CFRP	402.2	3.58	2000	151	44.7	137	0.16	161.6	0.19	146.8	0.17

Table A1 Database of tested eccentrically loaded FRP-RC columns (continued)

Ref.	Specimen's ID	Geometry						Main reinforcement					Concrete	Test results		Proposed		ACI CODE-440.11	
		l, mm	b, mm	h, mm	d, mm	λ	e/h	FRP type	A_f, mm^2	ρ_{ft}, %	f_{fu}, MPa	E_f, GPa	f'_c, MPa	P_{exp}, kN	$P_{exp.nor}$	P_{prop}	$P_{prop.nor}$	P_{ACI}	$P_{ACI.nor}$
	C12-T140-E0.5	1500	150	150	123	34.7	0.5	CFRP	226.2	2.01	2000	145	44.7	264	0.309	265.5	0.31	249.1	0.29
	C12-T140-E1.0	1500	150	150	123	34.7	1	CFRP	226.2	2.01	2000	145	44.7	129	0.151	137.6	0.16	129.5	0.15
	C12-T40-E0.5	1500	150	150	123	34.7	0.5	CFRP	226.2	2.01	2000	145	44.7	237.7	0.278	265.5	0.31	249.1	0.29
	C12-T40-E1.0	1500	150	150	123	34.7	1	CFRP	226.2	2.01	2000	145	44.7	113	0.132	137.6	0.16	129.5	0.15
Elmesalami, et al. [4]	B-16-40*	1100	180	180	135	22	0.22	BFRP	402.1	2.48	1242	49.3	28.4	577	0.738	444.7	0.57	432.7	0.55
	B-16-80	1100	180	180	135	22	0.44	BFRP	402.1	2.48	1242	49.3	34.4	347	0.366	270.3	0.29	261.4	0.28
	G-16-40*	1100	180	180	135	22	0.22	GFRP	402.1	2.48	785	44.9	28.4	585	0.748	443	0.57	432.4	0.55
	G-16-80	1100	180	180	135	22	0.44	GFRP	402.1	2.48	785	44.9	34.4	364	0.384	266.2	0.28	257.8	0.27
	B-20-40	1100	180	180	133	22	0.22	BFRP	628.3	3.88	913	45.9	34.4	720	0.76	540.7	0.57	523.6	0.55
	B-20-80	1100	180	180	133	22	0.44	BFRP	628.3	3.88	913	45.9	34.4	412	0.435	283.8	0.30	273.8	0.29
Karimi Pour, et al. [25]	N-G-60-50	1000	200	200	164	17.4	0.25	GFRP	760.3	3.8	966	39.5	37.3	1378	1.087	677.8	0.53	652.6	0.52
	N-G-60-100	1000	200	200	164	17.4	0.5	GFRP	760.3	3.8	966	39.5	36	631.1	0.516	346.5	0.28	329.1	0.27
	R-G-60-50	1000	200	200	164	17.4	0.25	GFRP	760.3	3.8	966	39.5	40.5	1532	1.112	732.5	0.53	706.2	0.51
	R-G-60-100	1000	200	200	164	17.4	0.5	GFRP	760.3	3.8	966	39.5	40	690	0.507	376.8	0.28	358.1	0.26
	N-G-120-50	1000	200	200	164	17.4	0.25	GFRP	760.3	3.8	966	39.5	35	1224	1.028	638.9	0.54	613.1	0.52
	N-G-120-100	1000	200	200	164	17.4	0.5	GFRP	760.3	3.8	966	39.5	35	605.4	0.509	339.1	0.28	321.7	0.27
	R-G-120-50	1000	200	200	164	17.4	0.25	GFRP	760.3	3.8	966	39.5	39	1311	0.989	706.8	0.53	681.5	0.51
	R-G-120-100	1000	200	200	164	17.4	0.5	GFRP	760.3	3.8	966	39.5	39	634.8	0.479	369.3	0.28	350.7	0.26
	N-G-180-50	1000	200	200	164	17.4	0.25	GFRP	760.3	3.8	966	39.5	36.2	1108	0.9	659	0.54	633.8	0.52
	N-G-180-100	1000	200	200	164	17.4	0.5	GFRP	760.3	3.8	966	39.5	36	592.5	0.484	346.5	0.28	329.1	0.27
	R-G-180-50	1000	200	200	164	17.4	0.25	GFRP	760.3	3.8	966	39.5	39.6	1173	0.871	716.9	0.53	691.2	0.51
	R-G-180-100	1000	200	200	164	17.4	0.5	GFRP	760.3	3.8	966	39.5	39	634.8	0.479	369.3	0.28	350.7	0.26
Mohammed S. Irhayyim, et al. [26]	C1-G	1700	150	150	125	39.4	0.67	GFRP	157.1	1.4	1207	50.3	26.1	131	0.262	95.6	0.19	90.8	0.18
	C2-G	1700	150	150	125	39.4	1	GFRP	157.1	1.4	1207	50.3	26.1	61	0.122	62.4	0.13	59.6	0.12
Hamid and Yousif [7]	31-2B10B150-40	1620	210	180	137	31.3	0.22	BFRP	402	2.13	978.6	48.26	38.5	754	0.61	695.5	0.56	683.1	0.55
	31-2B10B150-80	1620	210	180	137	31.3	0.44	BFRP	402	2.13	978.6	48.26	38.5	334	0.27	341.4	0.28	330.6	0.27
	31-2B10B150-120	1620	210	180	137	31.3	0.67	BFRP	402	2.13	978.6	48.26	38.5	170	0.137	212.2	0.17	205.1	0.17
	15-2B10B150-40	780	210	180	137	15.1	0.22	BFRP	402	2.13	978.6	48.26	38.5	772	0.624	695.5	0.56	683.1	0.55
	15-2B10B150-80	780	210	180	137	15.1	0.44	BFRP	402	2.13	978.6	48.26	38.5	395	0.319	341.4	0.28	330.6	0.27
	15-2B10B150-120	780	210	180	137	15.1	0.67	BFRP	402	2.13	978.6	48.26	38.5	182	0.147	212.2	0.17	205.1	0.17
Fathi, et al. [27]	G1	1200	150	150	125	27.8	0.27	GFRP	157	1.40	1000	40	30	335	0.654	251.6	0.49	244.9	0.48
	G2	1200	150	150	125	27.8	0.27	GFRP	157	1.40	1000	40	30	328	0.64	251.6	0.49	244.9	0.48
	G3	1200	150	150	125	27.8	0.27	GFRP	157	1.40	1000	40	30	320	0.625	251.6	0.49	244.9	0.48
Shakouri Mahmoudabadi, et al. [28]	50-E25	1200	180	180	155	23.1	0.14	GFRP	190	1.17	750	62.5	35	847.5	0.879	697.8	0.72	690.8	0.72
	100-E25	1200	180	180	155	23.1	0.14	GFRP	190	1.17	750	62.5	35	792.1	0.822	697.8	0.72	690.8	0.72
	50-E75	1200	180	180	155	23.1	0.42	GFRP	190	1.17	750	62.5	35	385.6	0.4	302.2	0.31	289.1	0.3
	100-E75	1200	180	180	155	23.1	0.42	GFRP	190	1.17	750	62.5	35	381.9	0.396	302.2	0.31	289.1	0.3
Sadat Hosseini and Sadeghian [29]	S20-e15	1220	203	203	170	20.9	0.15	GFRP	595.8	2.89	1020	53.7	32.5	865	0.76	820.1	0.72	790.8	0.7
	S40-e15	2440	203	203	170	41.7	0.15	GFRP	595.8	2.89	1020	53.7	32.5	588	0.517	820.1	0.72	790.8	0.7
	S40-e30	2440	203	203	170	41.7	0.3	GFRP	595.8	2.89	1020	53.7	32.5	558	0.49	539.7	0.47	512.1	0.45
Emam, et al. [30]	SC1	1500	250	250	220	20.8	0.2	GFRP	213.9	0.68	880	53.4	32.4	1018	0.591	1036.4	0.6	1026.9	0.6
	SC2	1500	250	300	270	17.4	0.17	GFRP	213.9	0.57	880	53.4	32.4	1321	0.64	1370.6	0.66	1366.6	0.66
	SC3	1500	250	350	320	14.9	0.14	GFRP	213.9	0.49	880	53.4	32.4	1731	0.718	1706.1	0.71	1709.2	0.71